

# Noise Spectroscopy Without Dynamical Decoupling Pulses

Arian Vezvaei,<sup>1,\*</sup> Nanako Shitara,<sup>1,2,\*</sup> Shuo Sun,<sup>2,3</sup> and Andrés Montoya-Castillo<sup>1,†</sup>

<sup>1</sup>*Department of Chemistry, University of Colorado Boulder, Colorado 80309, USA*

<sup>2</sup>*Department of Physics, University of Colorado Boulder, Colorado 80309, USA*

<sup>3</sup>*JILA, University of Colorado Boulder, Colorado 80309, USA*

Spectral characterization of noise environments that lead to the decoherence of qubits is critical to developing robust quantum technologies. While dynamical decoupling offers one of the most successful approaches to characterize noise spectra, it necessitates applying large sequences of  $\pi$  pulses that increase the complexity and cost of the method. Here, we introduce a noise spectroscopy method that utilizes only the Fourier transform of free induction decay measurements, thus removing the need for the application any  $\pi$  pulses. We show that our method faithfully recovers the correct noise spectra and outperforms previous dynamical decoupling schemes while significantly reducing its experimental overhead. We also discuss the experimental feasibility of our proposal and demonstrate its robustness in the presence of statistical measurement noise. Our method is applicable to a wide range of quantum platforms and provides a simpler path toward a more accurate spectral characterization of quantum devices, thus offering possibilities for tailored decoherence mitigation.

Nearly all current quantum technology applications rely on a two-level quantum system (qubit) that is subject to environmental noise. In the pure dephasing limit this environmental noise causes fluctuations in the frequency of the qubit that lead to decoherence. Spectral characterization of such environments is the most crucial step in successfully controlling and suppressing decoherence. Indeed, characterizing the noise spectrum allows for a filter-design approach that suppresses the noise and improves the coherence of the qubit [1–4]. Therefore, developing methods that can recover the noise spectrum of qubit environments has been one of the most active fields of research over the past two decades [5–8]. Among these efforts, dynamical decoupling noise spectroscopy (DDNS) [9–12] has been one of the most successful approaches. In this method, applying a sequence of  $\pi$ -pulses turns the qubit into a noise probe (approximated as a frequency comb) that isolates contributions from particular frequencies of the noise spectrum. The DD framework has been studied extensively theoretically and implemented experimentally in various platforms such as superconducting circuits [13, 14], ultracold atoms [15], quantum dots [16–18], and nitrogen-vacancy (NV) centers in diamonds [19, 20]. A DDNS protocol based on the Carr-Purcell-Meiboom-Gill (CPMG) sequence [21, 22] was proposed by Álvarez and Suter (AS) [9] which would ideally yield a system of equations and unknowns from the measured values of the qubit coherence  $C(t) = |\langle \rho_{01}(t) \rangle| / |\langle \rho_{01}(0) \rangle|$ , and specific frequencies of the spectrum. However, this method offers reasonable performance only when the number of  $\pi$ -pulses in each sequence is large. Beyond a pulse economy standpoint, other difficulties, such as deviations from the ideal frequency comb approximation [23], have recently inspired the development of a deep learning approach [24] to reconstruct the noise spectrum from the coherence function of the qubit. The success of this deep learning method suggests the existence of a one-to-one

mapping between the two quantities.

Here, we present a simple and inexpensive method that uniquely maps the measured coherence function of a qubit to its noise power spectrum, removing the need for long sequences of  $\pi$ -pulses at the heart of DDNS. Our approach only requires Free Induction Decay (FID) measurements of the qubit and employs a simple Fourier transform to accurately reconstruct the noise spectrum of the system. While Fourier spectroscopy has been implemented in Nuclear Magnetic Resonance and on different types of quantum processors [7, 25, 26], it has not been utilized in the context of pure dephasing with the filter function formalism. Here, we combine the Fourier transform technique with the filter function formalism to introduce an approach we call Fourier transform noise spectroscopy (FTNS) that significantly enhances one's ability to reconstruct the power spectrum while dramatically reducing the required experimental overhead.

We begin by laying out the theoretical basis for the filter function formalism in a pure dephasing setup [1, 6, 10, 27]. In this setup, the qubit relaxation process (quantified by  $T_1$ ) takes much longer than phase randomization (quantified by  $T_2^*$ ), implying that the decoherence time  $T_2^{-1} = (2T_1)^{-1} + T_2^{*-1} \approx T_2^{*-1}$  becomes a measure of how fast the phase information is lost due to environmental fluctuations. Frequency fluctuations of a qubit subject to a stationary, Gaussian noise,  $\beta(t)$ , can be described by the Hamiltonian  $\hat{H} = \frac{1}{2}[\Omega + \beta(t)]\hat{\sigma}_z$ , where  $\Omega$  is the natural frequency of the qubit. Here, the coherence function is  $C(t) = e^{-\chi(t)}$ , where the attenuation function  $\chi(t)$  is given by the overlap of the noise spectrum and a filter function that incorporates the effect of the pulses on the system [28]:

$$\chi(t) = -\ln[C(t)] = \frac{1}{4\pi} \int_{-\infty}^{\infty} d\omega S(\omega)F(\omega t). \quad (1)$$

The noise spectrum,  $S(\omega) = \int_{-\infty}^{\infty} dt e^{i\omega t} S(t)$ , is the Fourier transform of the equilibrium time correlation func-

tion of the environmental noise,  $S(t) = \langle \{\beta(t), \beta(0)\} \rangle / 2$ , where  $\{A, B\} = AB + BA$  is the anticommutator. The filter function,  $F(\omega t)$ , encodes the sign switching ( $\pm 1$ ) of the environmental fluctuations upon application of each  $\pi$  pulse in the sequence [1].

To demonstrate the advantages of our proposed FTNS, we first consider what is arguably the state-of-the-art approach to noise spectroscopy: the AS protocol. The main insight of the AS method lies in noting that when the number of pulses is sufficiently large, the filter function reaches the spectroscopic limit. In this limit, one can approximate the filter function by a  $\delta$ -function (frequency comb) with various harmonics:  $\chi(t) \approx t \sum_{0 < k < k_c} |A_{k\omega_0}|^2 S(k\omega_0)$ , where  $A_{k\omega_0}$  are the Fourier coefficients for a given pulse sequence, truncated at  $k_c$ . However, while applying many  $\pi$ -pulses allows the central peak to better resemble a  $\delta$ -function, it comes at the cost of increasing the number of harmonics in the frequency interval of interest. The extreme case of  $k_c = 1$  approximates the filter function as a single  $\delta$ -function, discarding many details of the noise spectrum. Often, one can still account for a limited number of harmonics (set by the cut-off  $k_c$ ), which attenuates the loss of spectral information [6, 24]. In the latter case, by appropriately varying the delay time between pulses and the total time of the sequence, one can form a linear system of equations consisting of coherence values at selected times and a matrix of contributing Fourier coefficients. Inverting this system of equations yields the noise spectrum at the probed frequencies, which are bounded by  $|\omega_{\max}^{\text{DDNS}}| \leq \pi/\tau$ . Here,  $\tau$  is the minimum delay between consecutive  $\pi$ -pulses required to minimize the overlap between subsequent pulses and validate the instantaneous pulse assumption. Furthermore, since  $A_{(k=0)} = 0$  for balanced pulse sequences like CPMG, the zero-frequency part of the spectrum cannot be accessed directly. Thus, going beyond the  $|\omega_{\max}^{\text{DDNS}}| \leq \pi/\tau$  limit and reading  $S(\omega = 0)$  requires *imbalanced* sequences such as Concatenated DD (CDD) [11]. Hence, the experimental overhead, frequency restrictions, and accuracy dependence on harmonic inclusions of AS [23] motivate the development of a more accessible scheme.

We introduce a radically more straightforward approach by inverting Eq. (1) directly to obtain the noise power spectrum, without the need for any  $\pi$ -pulses. Noting that for FID,  $F(\omega t) = (4/\omega^2) \sin^2(\omega t/2)$  [1], substituting  $F(\omega t)$  in Eq. (1), and differentiating both sides twice with respect to time, we obtain

$$\ddot{\chi}(t) = \frac{1}{2\pi} \int_{-\infty}^{\infty} d\omega S(\omega) \cos(\omega t). \quad (2)$$

Since  $S(-\omega) = S(\omega)$ , we Fourier transform both sides to find

$$S(\omega) = \sqrt{2\pi} \mathcal{F}[\ddot{\chi}(t)]. \quad (3)$$

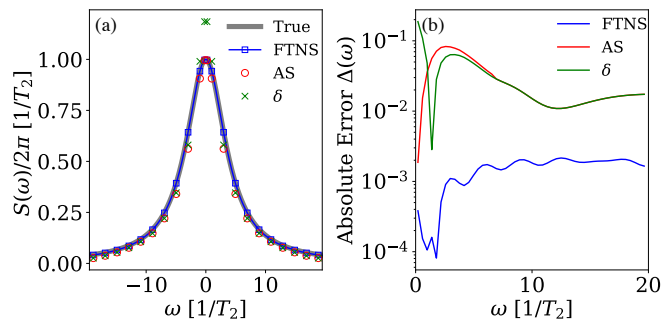


Figure 1. (a) A Lorentzian spectrum and its reconstruction using 2-pulse AS, the  $\delta$ -function approximation ( $k_c = 1$ ), and FTNS. One hundred frequencies have been reconstructed for the AS method, but only selected points have been marked for clarity. In the FTNS results, only frequencies corresponding to the marked AS ones are shown. (b) The absolute error compared to the true spectrum. While DDNS requires many pulses to achieve comparable accuracy, FTNS outperforms DDNS through using only FID measurements.

This straightforward derivation demonstrates that there is a simple and invertible one-to-one mapping between the noise power spectrum  $S(\omega)$  and the experimentally measured coherence function.

To illustrate this method for an analytically solvable case, we adopt a Gaussian-shaped noise power spectrum  $S(\omega) = Ae^{-(\omega/\sigma)^2}$ . The coherence function of this noise profile can be obtained analytically:

$$C(t) = \exp \left\{ -\frac{A}{\sigma} \left[ \frac{t\sigma}{2} \text{Erf} \left( \frac{t\sigma}{2} \right) + \frac{e^{-\frac{t^2\sigma^2}{4}} - 1}{\sqrt{\pi}} \right] \right\}, \quad (4)$$

where  $\text{Erf}(z) = 2\pi^{-1/2} \int_0^z e^{-x^2} dx$  is the Error function. The second derivative of the attenuation function takes the expected Gaussian form,  $\ddot{\chi}(t) = \frac{A}{\sqrt{2\pi}} e^{-\frac{t^2\sigma^2}{4}}$ , as does its Fourier transform,  $\mathcal{F} \left[ \frac{A}{\sqrt{2\pi}} e^{-\frac{t^2\sigma^2}{4}} \right] = \frac{A}{\sqrt{2\pi}} e^{-(\omega/\sigma)^2}$ , suggesting  $S_{\text{rec}}(\omega) = Ae^{-(\omega/\sigma)^2}$ . This illustrates that the FTNS method retrieves the original noise spectrum.

Translating the above insights into a NS procedure is straightforward. First, one measures the coherence function  $C(t)$  from FID by performing Ramsey measurements at various times, yielding an array of coherence values in  $[0, T_{\max}]$  with a sampling interval, or resolution,  $\delta t$ . One then takes a logarithm of the data and numerically performs a double derivative on the sampled  $\chi(t)$  values. A Fourier transform of the resulting data yields the noise spectrum  $S(\omega)$ . For this, one can employ a Discrete Fourier transform (DFT) or numerical quadrature to obtain equivalent results.

To illustrate the power of the FTNS approach, we assess its ability to reconstruct single- and double-Lorentzian spectra that are relevant to bulk [19] and near-surface [20] NV centers, respectively. Figure 1(a) shows a single Lorentzian peak (grey line) and its spectrum reconstruction using 2-pulse AS (red circles), the

$\delta$ -function approximation of 2-pulse AS (green crosses), and FTNS (blue line and squares), respectively [29]. The absolute error of the reconstructed spectrum compared to the true spectrum is computed as  $\Delta(\omega) = |S(\omega) - S_{\text{rec}}(\omega)|$ . As the figure demonstrates, FTNS outperforms the 2-pulse AS method while only requiring FID measurements.

Noting the difficulties of the DDNS approach in accessing the noise spectrum in both  $|\omega_{\text{max}}^{\text{DDNS}}| \leq \pi/\tau$  and  $S(\omega \rightarrow 0)$  limits, it is worth considering if and how similar limitations hinder the FTNS approach. Since our protocol for FTNS relies on the DFT, two quantities determine the highest accessible frequency ( $\omega_{\text{max}}^{\text{FTNS}}$ ) and its spectral resolution ( $\delta\omega^{\text{FTNS}}$ ), which also determines the lowest accessible frequency ( $\omega_{\text{min}}^{\text{FTNS}}$ ): the sampling interval,  $\delta t$ , of the coherence function measurement, and the total measurement time,  $T_{\text{max}}$ . Specifically,  $|\omega_{\text{max}}^{\text{FTNS}}| = \pi/\delta t$  and  $|\omega_{\text{min}}^{\text{FTNS}}| = \delta\omega = 1/T_{\text{max}}$ . While  $\delta t$  is determined by limitations of state-of-the-art measuring devices,  $T_{\text{max}}$  depends on the physical problem. Yet, for many cases of physical interest,  $\dot{\chi}(t) \rightarrow 0$  at times earlier than  $T_{\text{max}}$  [29], allowing one to zero-pad  $\dot{\chi}(t \geq T_{\text{max}})$  to a new effective  $\tilde{T}_{\text{max}} \gg T_{\text{max}}$ , offering sufficient spectral resolution to access  $S(\omega \rightarrow 0)$ .

Given the importance of  $\delta t$  in allowing FTNS to access high frequencies and the analogous role that the minimum delay time,  $\tau$ , plays in DDNS, we now consider their connection in greater detail.  $\tau$  determines the earliest time (after  $t = 0$ ) where one can measure the coherence function, i.e.,  $C(\tau)$ . Since the DFT requires measurements of  $C(t)$  at regular intervals, one might be tempted to assume that  $\delta t = \tau$ . However, this need not be the case. After all, for  $t \geq \tau$ , the measurement interval  $\delta t$  is not determined by  $\tau$  and can be set such that  $\delta t \ll \tau$ . While the resolution of the coherence function measurements at later times can be made as fine-grained as desired, one still needs to perform measurements in  $[0, \tau]$  to achieve a consistent  $\delta t$  through  $[0, T_{\text{max}}]$ . To achieve this, we suggest employing the limit  $\omega t \ll 1$ , which reveals that the attenuation function behaves as  $\chi(t) \approx \alpha t^2 + \beta t^4 + \gamma t^6$ , to fit  $C(t)$  at early times [29]. This guarantees that FTNS can be implemented even when constrained to the same minimum delay time of a DD pulse sequence.

We are now in a position to illustrate the ability of FTNS to capture spectra composed of a sum of Gaussians (Fig. 2(a)) and a double-Lorentzian (Fig. 2(b)), each compared to a reconstruction using 2-pulse AS subject to the same  $\tau$  constraint. In both panels, the reconstructed spectrum from 2-pulse AS (red circles) fails to capture the detailed structure within  $|\omega_{\text{max}}^{\text{DDNS}}| \leq \pi/\tau$  due to the limited number of DD pulses and cannot access  $|\omega| > \omega_{\text{max}}^{\text{DDNS}}$ . To go beyond these limits in DDNS, one can employ complex CDD sequences. In contrast, FTNS only encounters a difficulty in resolving the feature at  $\omega \sim \pm 3 [1/T_2]$  in Fig. 2(a) because we restrict

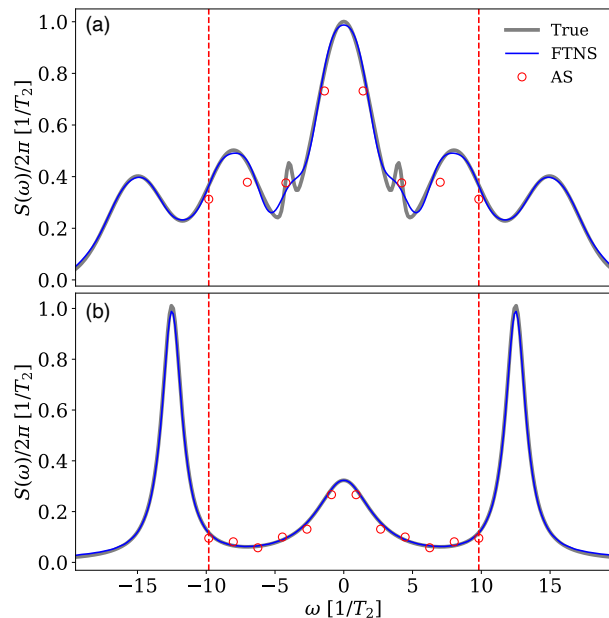


Figure 2. Examples of two structured noise spectra, reconstructed with FTNS (blue line) and a 2-pulse AS method (red circles): (a) A combination of four Gaussians and (b) a double Lorentzian. The red vertical lines indicate the frequency limits up to which the AS method can reconstruct the spectrum for the given minimum delay time:  $|\omega_{\text{max}}^{\text{DDNS}}| \leq \pi/\tau$ . Our FID-based FTNS reconstructs the noise spectrum to much higher accuracy both within, and beyond this frequency region.

$T_{\text{max}}$  such that  $C(t < T_{\text{max}}) \geq 0.005$  [29]. Thus, FTNS uses a simple FID measurement that successfully reconstructs the spectrum in the bounded frequency range and in higher frequency ranges, giving access to information that would be otherwise lost.

Since smaller  $\delta t$  gives access to higher  $\omega_{\text{max}}^{\text{FTNS}}$  but raises the cost of the experimental procedure, we turn to the trade-off in FTNS accuracy and the sampling interval  $\delta t$ . Figure 3 depicts FTNS spectrum reconstructions using sets of coherence measurements for a fixed measurement time  $T_{\text{max}}$  with varying  $\delta t$ . Clearly, increasing the resolution of coherence measurements (i.e., decreasing  $\delta t$ ) improves the accuracy of the FTNS reconstruction, especially at higher frequencies. As expected, even low sampling rates accurately reconstruct the low-frequency part of the spectrum while the high-frequency part can be systematically improved with finer  $\delta t$ . The ability of FTNS to capture the low-frequency component even at low sampling rates is particularly advantageous for decoherence mitigation purposes, as the low frequency noise often dominates decoherence [30, 31] [32]. Thus, even when measurement resolution is limited, FTNS can be expected to perform well at low frequencies and one can systematically assess its accuracy by checking convergence with finer  $\delta t$ .

Since FTNS requires performing two numerical derivatives, it is sensitive to measurement noise. There are

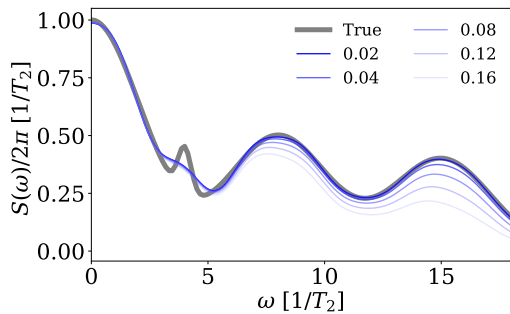


Figure 3. FTNS reconstructions of the multi-Gaussian spectrum in Fig. 2(a) for different values of the sampling interval,  $\delta t$ , for a fixed  $T_{\max}/T_2 = 10$ . The legend shows the values of  $\delta t/T_2$  used to obtain the FTNS results shown.

multiple sources of noise that can compromise the measured value of the coherence function at a given time. These include background and shot noises, and imperfect fidelity of the applied pulses [33, 34]. In optical setups, photon losses can also reduce the number of effective measurements. Nevertheless, various methods to perform controlled numerical derivatives of noisy data are available [35, 36]. As an example, here we utilize a simple denoising method that mitigates effect of noise and preserves all the advantages of FTNS even on structured noise spectra. Figure 4 shows examples of FTNS spectra reconstructed from artificially noisy data corresponding to an effective measurement error of 0.1%. We perform linear fitting of  $\chi(t)$  at late times and apply low-pass filters to recover the approximate noise spectrum, which shows good agreement with the actual spectrum, and reveals the essential features in the spectrum [29]. Therefore our simple FID-based NS approach can semiquantitatively recover the frequency and the height of the peaks of the noise spectrum, which constitute the minimum required spectral information to design effective filter functions to mitigate decoherence from a DD perspective.

While our analysis above accounts for theoretical constraints of the DFT, the experimental feasibility of FTNS is sensitive to  $\delta t$  and the minimum delay time  $\tau$ . Controlling these parameters requires flexibility in pulse design, which varies depending on the platform. For instance, solid-state spins can be controlled either optically with pulses that range from a few picoseconds up to 1 ns [37–40] or via a microwave with a pulse as short as 12 ns [41]. Such pulses allow for ns-scale minimum delay time  $\tau$  between pulses. Furthermore, tuning the sampling interval  $\delta t$  to ps-order precision is also achievable [42]. To illustrate how these timescales satisfy our FTNS requirements, consider the  $\delta t$  required to reconstruct the double-Lorentzian spectrum shown in Fig. 2(b) in the NV center parameter regime [19, 43–45] with  $T_2 = 1.32 \mu\text{s}$ . To obtain the accurate reconstruction shown in Fig. 2(b) one would need to measure 400 points with  $\delta t = 15 \text{ ns}$ . Thus,

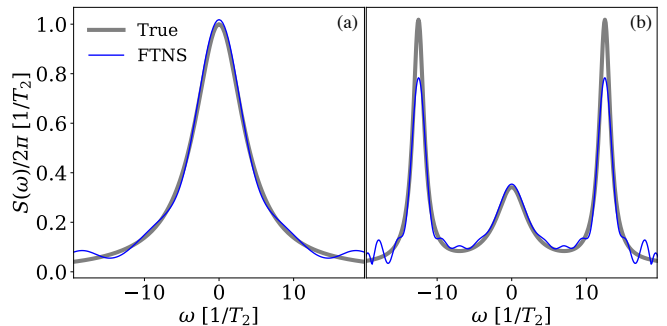


Figure 4. Spectrum reconstruction using FTNS assuming 0.1% measurement noise in coherence measurements for the same spectra shown in Figs. 1(a) and 2(b) in panels (a) and (b), respectively. Even subject to noisy data, utilizing simple denoising techniques allows FTNS to semiquantitatively capture the height and frequency of the peaks in the spectrum.

sufficiently high resolution measurements that faithfully reconstruct various noise spectra can be comfortably performed with experimentally available technology.

Since the feasibility of FTNS also relies on the ability to sufficiently reduce statistical noise ( $\sim 0.1\%$ ) within a reasonable time, we now consider what current technology can afford. Each point on the coherence curve arises from a Ramsey measurement at a given time, repeated multiple times to construct the ensemble average. Hence, to minimize statistical noise associated with finite sampling, the repetition rate of such experiments needs to be sufficiently high. We thus consider the time required on available experimental setups to bring the statistical error to the 0.1% value assumed in Fig. 4 in the measured coherence of NV centers with  $T_2 \sim \text{few } \mu\text{s}$  [19, 43, 44], with access to nanosecond microwave pulses. This 0.1% error requires that each point along the coherence curve be measured  $\sim 1 \times 10^6$  times. Here, a single measurement takes  $\sim 10 \mu\text{s}$  (including the initialization and readout). Thus, requiring  $\sim 100$  data points along  $C(t)$  takes  $\sim 2.8$  hours (assuming a modest photon collection rate of  $\sim 10\%$ ). Importantly, these numbers represent a conservative estimate and can be expected to improve significantly with better photon collection rates or through non-uniform sampling techniques [46–50]. Further, by requiring only two  $\pi/2$  pulses, FTNS avoids measurement noise arising from imperfect pulses, which accrues significantly in large DD pulse sequences with many  $\pi$ -pulses.

FTNS performs most efficiently when FID decays sufficiently slowly, as in trapped-ion systems [51, 52]. We have also developed a spin-echo FTNS protocol that unlocks fast decaying systems, allowing us to reconstruct even spectra dominated by strong inhomogeneous contributions, as in most NV centers [19, 20]. We introduce an iterative scheme to extract  $S(\omega)$  from our spin-echo FTNS in the supplementary materials [29].

In conclusion, we have introduced a novel noise spec-

troscopy method that significantly outperforms the current DDNS methods and is significantly easier to implement from both experimental and theoretical perspectives. Our work demonstrates the existence of a direct one-to-one invertible map between the pure dephasing coherence function within the filter function formalism and the noise power spectrum. Noting that current technology allows one to minimize measurement noise, it is clear that FTNS provides a promising route to accurately and inexpensively measure noise power spectra. Our FTNS proposal should be applicable to a wide range of quantum platforms and can be utilized as a powerful tool in deducing information about a qubit's environment.

*Acknowledgments:* A.M.C. acknowledges the start-up funds from the University of Colorado, Boulder. S.S. acknowledges funding from National Science Foundation (Grant No. 1734006 and 2016244).

---

\* These authors have contributed equally to this work.

† Andres.MontoyaCastillo@colorado.edu

- [1] L. Cywiński, R. M. Lutchyn, C. P. Nave, and S. Das Sarma, *Phys. Rev. B* **77**, 174509 (2008).
- [2] M. J. Biercuk, A. C. Doherty, and H. Uys, *Journal of Physics B: Atomic, Molecular and Optical Physics* **44**, 154002 (2011).
- [3] G. S. Uhrig, *Phys. Rev. Lett.* **98**, 100504 (2007).
- [4] M. J. Biercuk, H. Uys, A. P. VanDevender, N. Shiga, W. M. Itano, and J. J. Bollinger, *Physical Review A* **79** (2009), 10.1103/PhysRevA.79.062324.
- [5] W. Yang, Z.-Y. Wang, and R.-B. Liu, *Frontiers of Physics* **6** (2010), 10.1007/s11467-010-0113-8.
- [6] P. Szańkowski, G. Ramon, J. Krzywda, D. Kwiatkowski, and L. Cywiński, *Journal of Physics: Condensed Matter* **29**, 333001 (2017).
- [7] C. L. Degen, F. Reinhard, and P. Cappellaro, *Rev. Mod. Phys.* **89**, 035002 (2017).
- [8] D. Suter and G. A. Álvarez, *Rev. Mod. Phys.* **88**, 041001 (2016).
- [9] G. A. Álvarez and D. Suter, *Phys. Rev. Lett.* **107**, 230501 (2011).
- [10] T. Yuge, S. Sasaki, and Y. Hirayama, *Phys. Rev. Lett.* **107**, 170504 (2011).
- [11] L. M. Norris, G. A. Paz-Silva, and L. Viola, *Phys. Rev. Lett.* **116**, 150503 (2016).
- [12] J. Krzywda, P. Szańkowski, and L. Cywiński, *New Journal of Physics* **21**, 043034 (2019).
- [13] J. Bylander, S. Gustavsson, F. Yan, F. Yoshihara, K. Harrabi, G. Fitch, D. G. Cory, Y. Nakamura, J.-S. Tsai, and W. D. Oliver, *Nature Physics* **7**, 565 (2011).
- [14] Y. Sung, F. Beaudoin, L. Norris, F. Yan, D. Kim, J. Qiu, U. von Lüpke, J. Yoder, T. Orlando, S. Gustavsson, L. Viola, and W. Oliver, *Nature Communications* **10** (2019), 10.1038/s41467-019-11699-4.
- [15] I. Almog, Y. Sagi, G. Gordon, G. Bensky, G. Kurizki, and N. Davidson, *Journal of Physics B: Atomic, Molecular and Optical Physics* **44**, 154006 (2011).
- [16] O. E. Dial, M. D. Shulman, S. P. Harvey, H. Bluhm, V. Umansky, and A. Yacoby, *Phys. Rev. Lett.* **110**, 146804 (2013).
- [17] D. Farfurnik, H. Singh, Z. Luo, A. S. Bracker, S. G. Carter, R. M. Pettit, and E. Waks, ‘All-optical noise spectroscopy of a solid-state spin,’ (2021).
- [18] E. Connors, J. Nelson, L. Edge, and J. Nichol, *Nature Communications* **13** (2022), 10.1038/s41467-022-28519-x.
- [19] N. Bar-Gill, L. Pham, C. Belthangady, D. Sage, P. Cappellaro, J. Maze, M. Lukin, A. Yacoby, and R. Walsworth, *Nature communications* **3**, 858 (2012).
- [20] Y. Romach, C. Müller, T. Unden, L. J. Rogers, T. Isoda, K. M. Itoh, M. Markham, A. Stacey, J. Meijer, S. Pezzagna, B. Naydenov, L. P. McGuinness, N. Bar-Gill, and F. Jelezko, *Phys. Rev. Lett.* **114**, 017601 (2015).
- [21] H. Y. Carr and E. M. Purcell, *Phys. Rev.* **94**, 630 (1954).
- [22] S. Meiboom and D. Gill, *Review of Scientific Instruments* **29**, 688 (1958).
- [23] P. Szańkowski and L. Cywiński, *Phys. Rev. A* **97**, 032101 (2018).
- [24] D. F. Wise, J. J. Morton, and S. Dhomkar, *PRX Quantum* **2**, 010316 (2021).
- [25] F. Yan, J. Bylander, S. Gustavsson, F. Yoshihara, K. Harrabi, D. G. Cory, T. P. Orlando, Y. Nakamura, J.-S. Tsai, and W. D. Oliver, *Phys. Rev. B* **85**, 174521 (2012).
- [26] J. M. Boss, K. Chang, J. Armijo, K. Cujia, T. Rosskopf, J. R. Maze, and C. L. Degen, *Phys. Rev. Lett.* **116**, 197601 (2016).
- [27] B. Gu and I. Franco, *The Journal of Chemical Physics* **151**, 014109 (2019).
- [28] This form of filter-function formalism is the same for both classical and quantum noise models [10].
- [29] See the Supplementary Materials for figure parameters, an explicit derivation of the linear behavior at long times, a derivation of the early time behavior and its fitting procedure, the details of our denoising procedure, and an extension of the protocol to spin-echo sequence.
- [30] Y. Makhlin and A. Shnirman, *Journal of Experimental and Theoretical Physics Letters* **78**, 497 (2003).
- [31] J. Schrieff, Y. Makhlin, A. Shnirman, and G. Schön, *New Journal of Physics* **8**, 1 (2006).
- [32] Equation 1, subject to FID, suggests that a spectrum with a dominant low frequency component has a faster decoherence time. This is because the power spectrum is multiplied by  $\omega^2 F(\omega t) = \sin^2(\omega t/2)$ , which is sharply peaked at  $\omega = 0$ .
- [33] A. M. Tyryshkin, Z.-H. Wang, W. Zhang, E. E. Haller, J. W. Ager, V. V. Dobrovitski, and S. A. Lyon, ‘Dynamical decoupling in the presence of realistic pulse errors,’ (2010).
- [34] A. M. Souza, G. A. Álvarez, and D. Suter, *Phys. Rev. Lett.* **106**, 240501 (2011).
- [35] R. Chartrand, *ISRN Appl. Math.* **2011** (2011), 10.5402/2011/164564.
- [36] F. Van Breugel, J. N. Kutz, and B. W. Brunton, *IEEE Access* **8**, 196865 (2020).
- [37] D. Press, K. De Greve, P. McMahon, T. Ladd, B. Friess, C. Schneider, M. Kamp, S. Höfling, A. Forchel, and Y. Yamamoto, *Nature Photonics* **7**, 367 (2010).
- [38] A. Vezvae, E. Takou, P. Hilaire, M. Doty, and S. Economou, ‘Avoiding leakage and errors caused by unwanted transitions in lambda systems,’ (2022).

- [39] J. Bodey, R. Stockill, E. Denning, D. Gangloff, G. Éthier Majcher, D. Jackson, E. Clarke, M. Hugues, C. Gall, and M. Atatüre, *npj Quantum Information* **5** (2019), 10.1038/s41534-019-0206-3.
- [40] E. Takou and S. E. Economou, *Phys. Rev. B* **104**, 115302 (2021).
- [41] C. T. Nguyen, D. D. Sukachev, M. K. Bhaskar, B. Machielse, D. S. Levonian, E. N. Knall, P. Stroganov, C. Chia, M. J. Burek, R. Riedinger, H. Park, M. Lončar, and M. D. Lukin, *Phys. Rev. B* **100**, 165428 (2019).
- [42] Two microwave pulses with a controllable delay can be generated with an arbitrary waveform generator. The sampling rate of the best commercial arbitrary waveform generators can exceed 100 GS/s (i.e., a delay resolution of 10 ps is possible). The delay between two optical pulses can be easily controlled by varying the length of an arm in the Michelson Interferometer. A delay of 1 ps corresponds to a change of  $\sim 0.3$  mm in the arm length, which can be easily achieved with commercial translational stages.
- [43] E. Bauch, C. A. Hart, J. M. Schloss, M. J. Turner, J. F. Barry, P. Kehayias, S. Singh, and R. L. Walsworth, *Phys. Rev. X* **8**, 031025 (2018).
- [44] E. Bauch, S. Singh, J. Lee, C. A. Hart, J. M. Schloss, M. J. Turner, J. F. Barry, L. M. Pham, N. Bar-Gill, S. F. Yelin, and R. L. Walsworth, *Phys. Rev. B* **102**, 134210 (2020).
- [45] J. M. Taylor, P. Cappellaro, L. Childress, L. Jiang, D. Budker, P. R. Hemmer, A. Yacoby, R. Walsworth, and M. D. Lukin, *Nature Physics* **4**, 810 (2008).
- [46] J. Fessler and B. Sutton, *IEEE Transactions on Signal Processing* **51**, 560 (2003).
- [47] L. D’Addario and S. Wernecke, *IEEE Transactions on Computers* **26**, 351 (1977).
- [48] K. Kazimierczuk, M. Misiak, J. Stanek, A. Zawadzka-Kazimierczuk, and W. Koźmiński, *Topics in current chemistry* **316**, 79 (2011).
- [49] D. Holland, M. Bostock, L. Gladden, and D. Nietlispach, *Angewandte Chemie (International ed. in English)* **50**, 6548 (2011).
- [50] V. Jaravine, I. Ibragimov, and V. Orekhov, *Nature methods* **3**, 605 (2006).
- [51] C. D. Bruzewicz, J. Chiaverini, R. McConnell, and J. M. Sage, *Applied Physics Reviews* **6**, 021314 (2019), <https://doi.org/10.1063/1.5088164>.
- [52] T. Ruster, C. T. Schmiegelow, H. Kaufmann, C. Warschburger, F. Schmidt-Kaler, and U. G. Poschinger, *Applied Physics B* **122** (2016), 10.1007/s00340-016-6527-4.

# Supplementary Material: Noise Spectroscopy Without Dynamical Decoupling Pulses

Arian Vezvaei,<sup>1</sup> Nanako Shitara,<sup>1,2</sup> Shuo Sun,<sup>2,3</sup> and Andrés Montoya-Castillo<sup>1,\*</sup>

<sup>1</sup>*Department of Chemistry, University of Colorado Boulder, Colorado 80309, USA*

<sup>2</sup>*Department of Physics, University of Colorado Boulder, Colorado 80309, USA*

<sup>3</sup>*JILA, University of Colorado Boulder, Colorado 80309, USA*

In Sec. I, we summarize the parameters and short-time fitting procedure for the attenuation function,  $\chi(t)$ , used for all figures in the main text. In Sec. II, we demonstrate that two physically inspired examples of power spectra—Lorentzian and Gaussian spectra—lead to long-time linear behavior in  $\chi(t)$ . In Sec. III, we outline the denoising procedure we applied in Fig. 4 of the main text.

## I. FIGURE PARAMETERS AND EARLY TIME MEASUREMENT FITTING

Here we report the parameters that we have used for the figures in the main text. However, before turning to each figure, we first detail the fitting procedure we employed to access the short-time values of the coherence function,  $C(t)$ , when the measurement resolution was smaller than the minimum delay time of the  $\pi/2$  pulses, i.e.,  $\delta t < \tau$ .

As discussed in the main text, since our sampling interval  $\delta t$  is smaller than the minimum delay time  $\tau$ , we obtain effective coherence function measurements at early times  $[0, \tau]$  by employing the small  $\omega t$  limit of the free induction decay attenuation function,  $\chi(t)$ . For early times (i.e., when  $\omega t \ll 1$ ), one can expand  $\chi(t)$  as

$$\begin{aligned}\chi(t) &= \frac{1}{\pi} \int_{-\infty}^{\infty} d\omega \frac{1}{\omega^2} S(\omega) \sin^2\left(\frac{\omega t}{2}\right) \\ &\approx \frac{1}{\pi} \int_{-\infty}^{\infty} d\omega \frac{1}{\omega^2} S(\omega) \left[ \frac{(\omega t)^2}{2^2} - \frac{(\omega t)^4}{2^4 \cdot 3} + \frac{2(\omega t)^6}{2^6 \cdot 45} \right] \\ &\equiv \alpha t^2 + \beta t^4 + \gamma t^6,\end{aligned}\tag{S1}$$

where

$$\alpha = \frac{1}{2^2 \pi} \int_{-\infty}^{\infty} d\omega S(\omega),\tag{S2a}$$

$$\beta = \frac{1}{2^4 \cdot 3 \pi} \int_{-\infty}^{\infty} d\omega \omega^2 S(\omega),\tag{S2b}$$

$$\gamma = \frac{1}{2^5 \cdot 45 \pi} \int_{-\infty}^{\infty} d\omega \omega^4 S(\omega),\tag{S2c}$$

correspond to the integral over the power spectrum and its first two moments. Since one does not have access to  $\{\alpha, \beta, \gamma\}$  a priori, we employ a polynomial fitting procedure subject to the functional form in Eq. (S1) to obtain values for the attenuation function,  $\chi(t)$ , over the interval  $[0, \tau]$ . To ensure physically correct behavior for the interpolated  $\chi(t)$  in the short-time region, we employ two additional fitting constraints:  $C(t \rightarrow 0) = 1$  and in the region at and beyond  $\tau$ , the fitting procedure must align with the first few measured values. Thus, we perform the polynomial fitting in the interval  $[0, \tau + \epsilon]$  where  $\epsilon$  contains the first few points accessible via direct measurement of the coherence curve. This ensures that the inferred values of these constants are correctly reconstructing the expected coherence curve well into the  $\epsilon$  interval that one can directly measure. We expect that, depending on the structure of the noise and the resulting coherence function, one might need keep more terms in the expansion above to be able to infer the points in the  $[0, \tau + \epsilon]$  interval in future applications.

The values of the early time parameters, as well as the spectrum parameters of each figure from the main text, are as follows:

1. Figure 1: the spectrum corresponds to a single Lorentzian

$$S(\omega) = \frac{s_0}{1 + (8\omega/\omega_c)^2},\tag{S3}$$



where  $s_0 = 2\pi/T_2$  and  $\omega_c = 32/T_2$ . The coherence function used to implement our Fourier transform noise spectroscopy (FTNS) protocol contained 100 points with a resolution of  $\delta t/T_{\max} = 0.01$  ( $T_{\max}/T_2 = 2.2$ ), where  $T_{\max}$  is the total measurement time. Notice that throughout our examples, we set these total measurements time such that the coherence value does not become less than  $C(t) = 0.005$ . This ensures that the measured values remain within the reasonable experimentally accessible range. The parameters obtained from the early-time fitting are  $\{\alpha, \beta, \gamma\} = \{5.3, -10.2, 0.0\}$ .

2. Figure 2(a): the spectrum corresponds to a double-Lorentzian,

$$S(\omega) = \frac{s_0}{1 + (8\omega/\omega_c)^2} + \frac{s_1}{1 + 2(16[\text{sgn}(\omega)\omega - d]/\omega_c)^2}, \quad (\text{S4})$$

where  $s_0 = 2/T_2$ ,  $\omega_c = 20/T_2$ ,  $d = 12.5/T_2$ , and  $s_1 = 2\pi/T_2$ . The coherence function used to implement our FTNS protocol contained 400 points with a resolution of  $\delta t/T_{\max} = 0.0025$  ( $T_{\max}/T_2 = 4.1$ ). The parameters obtained from the early-time fitting are  $\{\alpha, \beta, \gamma\} = \{3.4, -19.7, 0.0\}$

3. Figure 2(b): the spectrum corresponds to a sum of four Gaussians

$$S(\omega) = \sum_i A_i e^{-(\omega - \mu_i)^2 / \sigma_i^2}, \quad (\text{S5})$$

where  $A_i \in \{1.0, 0.2, 0.4, 0.5\}2\pi/T_2$ ,  $\sigma_i \in \{3.0, 0.4, 3.0, 3.0\}/T_2$ , and  $\mu_i \in \{0.0, 0.4, 15.0, 8.0\}/T_2$ . The coherence function used to implement our FTNS protocol contained 300 points with a resolution of  $\delta t/T_{\max} = 0.0033$  ( $T_{\max}/T_2 = 3.4$ ). The parameters obtained from the early-time fitting are  $\{\alpha, \beta, \gamma\} = \{7.5, -47.9, 173.0\}$ .

4. Figure 3: all parameters are the same as for Fig. 2(b).

5. Figure 4: the parameters for Fig. 4(a) and Fig. 4(b) are the same as for Fig. 1(a) and Fig. 2(a), respectively.

In all cases, we employed a minimum delay time such that  $\tau/\delta t = 16$  for both FTNS and dynamical decoupling noise spectroscopy (DDNS).

## II. LINEAR BEHAVIOR OF $\chi(t)$ AT LONG TIMES

In this section we explicitly show that  $\chi(t)$  behaves linearly at  $t \rightarrow \infty$  for the Lorentzian and the Gaussian spectra, which are two commonly encountered spectral shapes. We also demonstrate that  $\ddot{\chi}(t) \rightarrow 0$  at  $t \rightarrow \infty$ . To do this, we consider a generic form for  $S(\omega)$  and obtain an expression for  $\chi(t)$ . The  $t \rightarrow \infty$  behavior of this  $\chi(t)$  reveals whether the proposed linear fitting is appropriate.

### Lorentzian spectrum

We first consider a Lorentzian spectrum:

$$S(\omega) = A \left( \frac{1}{1 + \left(\frac{\omega-d}{\omega_c}\right)^2} + \frac{1}{1 + \left(\frac{\omega+d}{\omega_c}\right)^2} \right). \quad (\text{S6})$$

This form ensures that it is symmetric. Taking the inverse Fourier transform of  $S(\omega)/\sqrt{2\pi}$ , we obtain,

$$\ddot{\chi}(t) = A\omega_c e^{-t\omega_c} \cos(dt). \quad (\text{S7})$$

Clearly, this is a function that decays exponentially to zero at long times. From this we can obtain  $\dot{\chi}(t)$  and  $\chi(t)$ :

$$\dot{\chi}(t) = \frac{A\omega_c e^{-t\omega_c} (d \sin(dt) - \omega_c \cos(dt))}{d^2 + \omega_c^2} + C_1, \quad (\text{S8a})$$

$$\chi(t) = \frac{A\omega_c e^{-t\omega_c} ((\omega_c^2 - d^2) \cos(dt) - 2d\omega_c \sin(dt))}{(d^2 + \omega_c^2)^2} + C_1 t + C_2, \quad (\text{S8b})$$



where  $C_1$  and  $C_2$  are integration constants, which we can find by enforcing the appropriate boundary conditions. The coherence should start at 1 at  $t = 0$ , so we expect  $\chi(t = 0) = 0$ . We can also examine the boundary condition for  $\dot{\chi}(t)$ :

$$\dot{\chi}(t) = \frac{1}{\pi} \int_{-\infty}^{\infty} d\omega \frac{S(\omega)}{\omega} \sin\left(\frac{\omega t}{2}\right) \cos\left(\frac{\omega t}{2}\right), \quad (\text{S9})$$

which implies that  $\dot{\chi}(t = 0) = 0$ . We impose these by evaluating  $\dot{\chi}(0)$  and  $\chi(0)$ :

$$\dot{\chi}(0) = -\frac{A\omega_c^2}{d^2 + \omega_c^2} + C_1 = 0 \quad (\text{S10})$$

$$\chi(0) = \frac{A\omega_c (\omega_c^2 - d^2)}{(d^2 + \omega_c^2)^2} + C_2 = 0. \quad (\text{S11})$$

Hence,

$$\chi(t) = \frac{A\omega_c e^{-t\omega_c} ((\omega_c^2 - d^2) \cos(dt) - 2d\omega_c \sin(dt))}{(d^2 + \omega_c^2)^2} + \frac{A\omega_c^2}{d^2 + \omega_c^2} t - \frac{A\omega_c (\omega_c^2 - d^2)}{(d^2 + \omega_c^2)^2}, \quad (\text{S12})$$

and we indeed see that the long-time limit of the attenuation function is a linear function in  $t$ ,

$$\lim_{t \rightarrow \infty} \chi(t) = \frac{A\omega_c^2}{d^2 + \omega_c^2} t - \frac{A\omega_c (\omega_c^2 - d^2)}{(d^2 + \omega_c^2)^2}. \quad (\text{S13})$$

### Gaussian spectrum

One can perform a similar analysis for a Gaussian spectrum,

$$S(\omega) = A \exp\left\{-\left(\frac{\omega - d}{\sigma}\right)^2\right\} + A \exp\left\{-\left(\frac{\omega + d}{\sigma}\right)^2\right\}. \quad (\text{S14})$$

We can again take the inverse Fourier transform of  $S(\omega)/\sqrt{2\pi}$  to obtain,

$$\ddot{\chi}(t) = \frac{A}{2\sqrt{\pi}} |\sigma| \exp\left\{-\frac{1}{4}t(4id + t\sigma^2)\right\} (1 + e^{2idt}), \quad (\text{S15})$$

which goes to zero at long times. We can integrate Eq. (S15) to obtain expressions for  $\dot{\chi}(t)$  and  $\chi(t)$  subject to their constraints at  $t \rightarrow 0$ , i.e.,  $\chi(0) = 0$  and  $\dot{\chi}(0) = 0$ :

$$\begin{aligned} \dot{\chi}(t) &= A e^{-\frac{d^2}{\sigma^2}} \operatorname{Re}\left(\operatorname{Erf}\left(\frac{id}{\sigma} + \frac{\sigma t}{2}\right)\right) \\ \chi(t) &= -\frac{2A\left(\sigma + ie^{-\frac{d^2}{\sigma^2}}\sqrt{\pi}d \operatorname{Erf}\left(\frac{id}{\sigma}\right)\right)}{\sqrt{\pi}\sigma^2} + \operatorname{Re}\left(\frac{Ae^{-\frac{d^2}{\sigma^2}}\left(2\sigma e^{\left(\frac{d}{\sigma} + \frac{i\sigma t}{2}\right)^2} + i\sqrt{\pi}(2d + i\sigma^2 t) \operatorname{Erf}\left(\frac{id}{\sigma} - \frac{\sigma t}{2}\right)\right)}{\sqrt{\pi}\sigma^2}\right) \end{aligned} \quad (\text{S16a})$$

where  $\operatorname{Re}(\cdot)$  denotes the real part, and  $\operatorname{Erf}(\cdot)$  is the error function. Noting that  $\lim_{t \rightarrow \infty} \operatorname{Erf}(t) \rightarrow 1$ , it is clear that the long-time limit of the attenuation function becomes,

$$\lim_{t \rightarrow \infty} \chi(t) = \frac{A}{\sigma^2} \left( e^{-\frac{d^2}{\sigma^2}} \left( -2id \operatorname{Erf}\left(\frac{id}{\sigma}\right) + \sigma^2 t \right) - \frac{2\sigma}{\sqrt{\pi}} \right). \quad (\text{S17})$$

Therefore, we have shown here that for a Gaussian-shaped power spectrum, a long-time linear behavior of  $\chi(t)$  is also expected.

### III. MEASUREMENT NOISE MITIGATION PROTOCOL

Here we outline the details of our approach to mitigate noisy measurements. In particular, we detail the protocol we developed and employed to generate Fig. 4 from noisy coherence measurements. As a demonstration, we have used *Mathematica*, but our protocol is general and can be implemented within other computational softwares. We emphasize that this is *one example* of a denoising protocol; other procedures may be more appropriate for different data and physical problems.

In Fig. 4, we model the noise in the coherence function as arising from a normal distribution with mean 0 and standard deviation 0.001 at each measurement point. The noise has been adjusted such that for early times, the acquired value for  $C(t)$  does not exceed unity, and at later times it does not fall below zero.

We now summarize our denoising protocol:

1. Mirror the coherence data around  $t = 0$  to get an effective coherence profile from  $-T_{\max}$  to  $T_{\max}$ . This allows the numerical time-derivative to obtain a better value of  $\chi(t)$  at  $t = 0$ , which helps to improve the performance of the Fourier transform near  $\omega = 0$ .
2. Process the noisy coherence data through a low-pass filter, with the cutoff frequency set to half of the sampling rate. All instances of the low-pass filter are implemented using the Mathematica built-in `LowpassFilter`.
3. Take the logarithm of the smoothed coherence to get effective  $\chi(t)$  values.
4. Plot the resulting data to visually discern whether the late time behavior appears linear and within what range a linear fit appears suitable. In this case, we determined that linear fits from  $t/T_{\max} = 0.45$  to  $t/T_{\max} = 0.75$  for Fig. 4(a) and from  $t/T_{\max} = 0.5$  to  $t/T_{\max} = 0.8$  for Fig. 4(b) were appropriate. The justification for this linear fitting at long times is given in Sec. II of this SM.
5. Perform a linear fit on the ranges selected. We employed the `Fit` function in Mathematica.
6. Replace the data within the selected range with the linear fit. This leads to a modified  $\chi(t)$ , which we denote by  $\tilde{\chi}(t)$ .
7. *Optional:* After applying a linear fit, one can extend the  $\chi(t)$  data to arbitrarily long times, which results in a longer effective measurement time, which in turn provides improved resolution in frequency space of the FTNS approach. This step was not implemented in the generation of Fig. 4 in the main text and its implementation would only increase the frequency resolution of the spectrum.
8. Perform a numerical time derivative of  $\tilde{\chi}(t)$ . To obtain the numerical time derivatives, we implemented first order forward and backward difference approximation on the first and last data points, and a second order centered-difference approximation on the rest of the points. This is the algorithm behind various differentiation packages, such as `numpy.gradient`, which we used for the simulations in Figs. 1, 2, and 3 in the main text.
9. If the linear fitting causes a discontinuity, we remove its effect on the derivative by setting the value of the first derivative at the discontinuity to the derivative of the linear fit.
10. Apply another low-pass filter at a cutoff frequency at 1/4 of the sampling rate.
11. We take a second numerical time-derivative of the data.
12. We apply a Fourier transform on the data as discussed in the main text: one can, for example, use any FFT implementation available in numerical packages (e.g., `numpy`) or implement the Fourier transform manually by performing an integral of the quantity  $\tilde{\tilde{\chi}}(t)e^{i\omega t}/\sqrt{2\pi}$  over time, where the integration is approximated by the trapezoidal rule without changing the result.
13. For the Fourier transform, we employed a frequency range from  $\pm$  half of the sampling rate of the coherence, with  $\delta t/T_{\max} = 0.002$  ( $\delta t/T_{\max} = 0.01$ ) for Fig. 4(b) (Fig. 4(a)). Finally, this is divided by  $\sqrt{2\pi}$  to obtain the denoised spectra seen in Fig. 4.

We can study the performance of FTNS using this particular denoising protocol at various effective measurement noise percentages. Figure S1 gives examples of this for the two spectra used Fig. 4 in the main text at effective noise values of 1.0%, 0.5%, and 0.1%. As expected, lower noise values give better agreement with the true spectrum. Yet, the agreement between FTNS and the true spectrum demonstrates that FTNS is able to robustly capture the major

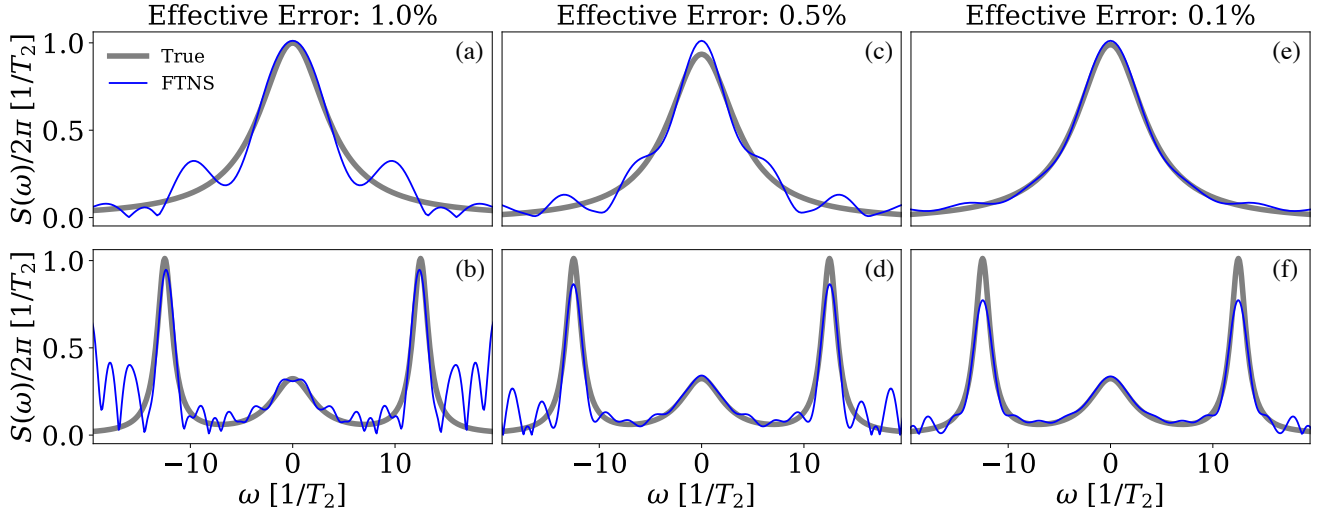


Figure S1. FTNS in the presence of various effective measurement noise, for the two examples demonstrated in Fig. 4. Specifically, the noise levels for the panels are 1.0% for (a) and (b), 0.5% for (c) and (d), and 0.1% for (e) and (f). While performance improves for lower effective noise, the peaked spectral features remain more or less robust under all three cases.

peaks in the spectrum in all cases. Strikingly, the artifacts of the Fourier transform of noisy data, which are most prominent in the examples with 1.0% noise levels, systematically decrease with increased sampling. Thus, to robustly identify features of the true spectrum in an experimental implementation of FTNS, it would be helpful to compare averages of smaller batches of measurements for common peaked features that appear consistently. Such comparisons can also be used to check the convergence of the reconstructed spectrum as a function of the extent of averaging done during the measurement process.

#### IV. SPIN-ECHO FTNS

As we mention in the main text, the FTNS protocol requires FID coherence measurements that decay sufficiently slowly so as to allow enough measurements of the coherence curve to support a well-behaved Fourier transform. A fast decaying behavior could be caused by a sharply peaked low-frequency noise component at  $\omega = 0$ . In such scenarios one can utilize a single  $\pi$ -pulse (a Spin-Echo (SE) sequence) to remove the effect of the low-frequency component of  $S(\omega)$  to prolong the  $T_2$  time. Therefore it would be beneficial to provide a one-to-one map and a noise spectroscopy protocol to perform FTNS based on the SE sequence.

The filter function of the SE sequence is given as  $F(\omega, t) = (16/\omega^2) \sin(\omega t/4)^4$ . Following similar steps to those done for the FID, we take a double derivative of the SE attenuation function to find,

$$\ddot{\chi}_{SE}(t) = \frac{1}{2\pi} \int_{-\infty}^{\infty} d\omega S(\omega) [\cos(\omega t/2) - \cos(\omega t)], \quad (\text{S18})$$

and therefore,

$$\sqrt{2\pi} \mathcal{F}[\ddot{\chi}_{SE}(t)] = 2M(2\omega), \quad (\text{S19})$$

where,  $M(\omega) \equiv S(\omega) - S(\omega/2)/2$  and corresponds to an array of measurements that one can make in the lab at regular values of  $\omega_n \in [0, \delta\omega, 2\delta\omega, \dots, n_{\max}\delta\omega]$ , where  $n \in \mathbb{N}$ , separated by an interval  $\delta\omega$  that are accessible via the Fourier transform of the second derivative of the SE coherence function. Hence, we write  $M(\omega_n) = M(n \times \delta\omega)$ .

While the map in Eq. (S19) provides the spectral function  $S(\omega)$ , it also contains an unwanted part  $S(2\omega)$  which we need to remove from our FT results. Here we provide a simple and effective recursive method that allows us to extract the spectral function  $S(\omega)$  from our SE-based FTNS results:

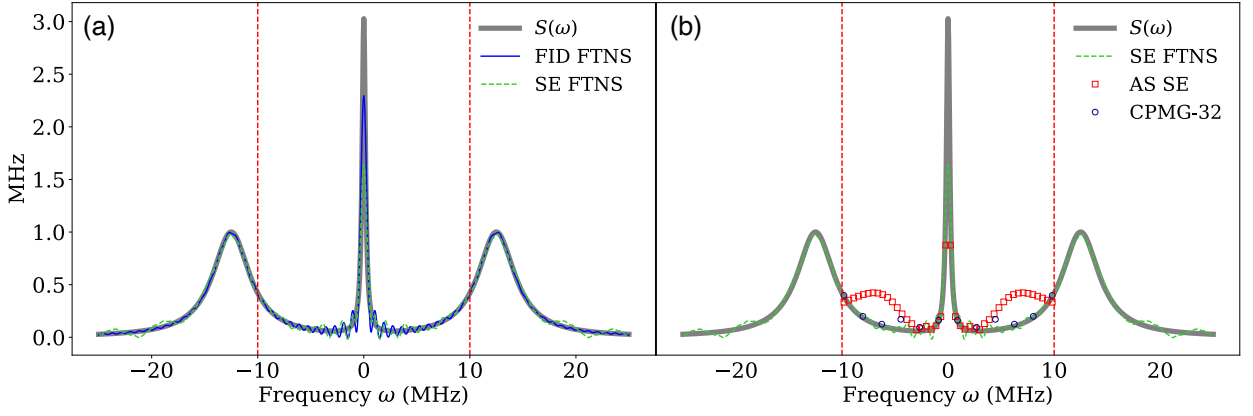


Figure S2. (a) Performance of SE and FID FTNS for a very sharply peaked low-frequency double-Lorentzian spectrum. (b) Comparison of SE FTNS reconstruction, and SE and CPMG-32 pulse-sequence DDNS. While the FTNS method recovers much of the low-frequency and and high-frequency components, the DDNS methods fail to capture the high-frequency information and also miss the central peak as applying DD pulses remove the information about such a peak.

$$S(2n\delta\omega) = M(2n\delta\omega) + \frac{1}{2}S(n\delta\omega), \quad (\text{S20})$$

$$S((2n+1)\delta\omega) = M((2n+1)\delta\omega) + \frac{1}{4}(S((n+1)\delta\omega) + S(n\delta\omega)). \quad (\text{S21})$$

To arrive at this result, we first exploit the fact that  $S(0) = 2M(0)$ . While the Fourier transform will not give access to  $M(\omega = 0)$ , it can be interpolated. We then make an approximation for  $S(n\delta\omega/2)$  for odd  $n$  as the arithmetic average of two adjacent points:  $S(n\delta\omega/2) \approx (1/2)(S((n-1)\delta\omega/2) + S((n+1)\delta\omega/2))$ . This allows us to find  $S(\delta\omega) = (4/3)(M(\delta\omega) - S(0)/4)$ .

To see the performance of the SE version of the FTNS, we apply this protocol to an example of highly peaked low-frequency double-Lorentzian spectrum from Eq. (S4). Specifically, we select a sharp central peak relevant to NV centers, corresponding to sample 2 from Reference [20] of the main text. (This corresponds to setting  $s_0 = 3$  (MHz),  $\omega_c = 1.5$  (MHz),  $d = 12.5$  (MHz), and  $s_1 = 1$  (MHz), in the parameter regime of NV centers.) In Fig. S2 we show the performance of SE FTNS and have compared it to both FID FTNS and DDNS. In Fig. S2(a) we see that while both FTNS methods perform equally well in reconstructing the high frequency components of the spectrum, FID FTNS does a better job at reconstructing the low frequency components. This is because when we apply a single  $\pi$ -pulse, it removes information about the structure of the low-frequency component. In Fig. S2(b) we observe that the DDNS methods are still limited in the reconstruction of higher frequencies. Thus, both FID and SE FTNS perform better than DDNS, capturing an informative description of both the central peak, and also the higher frequency components, which are inaccessible under DDNS.

Here we conclude the comparison of both versions of FTNS and state-of-the-art DDNS by making a few general remarks regarding the applicability of both methods. First, the information about the strong low-frequency component peak is only available at long times of the coherence function  $C(t)$ . Since one cannot measure arbitrary small values of the coherence function  $C(t)$  at long times, we set a measurement cut-off of  $C(t) < 0.005$  for both methods, which aligns with the estimate of measurement errors given in Section III. This limits the number of points that can be reconstructed via DDNS and can also lead to numerical instability of the FT. While for the DDNS method, this can lead to poor resolution of the reconstructed spectrum, as is seen for the CPMG-32 case in Fig. S2 (b), for the FTNS can recover the prominent features of the noise spectrum, albeit at the cost of introducing unphysical oscillations, that can be tamed with more extensive measurements. Second, while it is possible to invert higher-order DD sequences via the FTNS method and extract the noise power spectrum from the resulting FT via a similar iterative approach as that outlined above, we observe that the FID and SE perform equally well. Thus, while the accuracy of DDNS method requires larger number of pulses, for the FTNS method, FID and SE suffice. Indeed, we would only need to resort to SE measurements for fast decaying systems. Otherwise, simple FID measurements will provide the same spectral information. Therefore, even for systems whose FID coherence decays rapidly, we envision FTNS to be a noise spectroscopy method which still offers advantages in terms of resolution and simplicity of implementation.